ACS OMEGA

http://pubs.acs.org/journal/acsodf

Article

Biowaste Eggshell Membranes for Bio-triboelectric Nanogenerators and Smart Sensors

Meng-Fang Lin,* Po-Yen Chang, Chia-Hsien Lee, Xin-Xian Wu, Ru-Jong Jeng, and Chih-Ping Chen*

Cite This: *ACS Omega* 2023, 8, 6699−6707

Read Online

ACCESS | Metrics & More | Article Recommendations | Supporting Information

ABSTRACT: In this study, we used a simple and cost-effective method to fabricate triboelectric nanogenerators (TENGs) based on biowaste eggshell membranes (EMs). We prepared stretchable electrodes with various types of EMs (hen, duck, goose, and ostrich) and employed them as positive friction materials for bio-TENGs. A comparison of the electrical properties of the hen, duck, goose, and ostrich EMs revealed that the output voltage of the ostrich EM could reach up to 300 V, due to its abundant functional groups, natural fiber structure, high surface roughness, high surface charge, and high dielectric constant. The output power of the resulting device reached 0.18 mW, sufficient to power 250 red light-emitting diodes simultaneously, as well as a digital watch. This device also displayed good durability when subjected to 9000 cycles at 30 N at a frequency of 3 Hz. Furthermore, we designed an ostrich EM-TENG as a smart sensor for the detection of body motion, including leg movement and the pressing of different numbers of fingers.

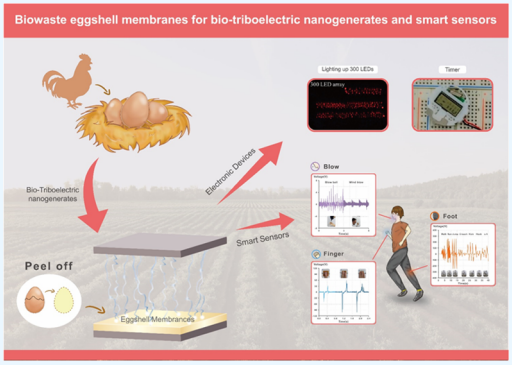

INTRODUCTION

The drive to replace traditional fossil fuels with sustainable and renewable energy sources has grown rapidly in the past decade, due to possible energy crises and higher standards for environmental protection. As a consequence, natural and green energy sources, including solar, wind, and water, have attracted much research interest in the pursuit of sustainable and renewable energy.[1−4] At the same time, with rapid progress in the Internet of Things (IoT), smart and portable electronic products have become essential parts of our daily lives, leading to a steadily growing demand for independent power sources detached from the power grid.[5] Nevertheless, accommodating conventional rigidly structured portable power sources without the self-charging ability (particularly batteries and supercapacitors) limits the potential design space for electronic devices. Hence, there is a great desire to develop sustainable and flexible energy harvesting technologies that can convert ambient energy into valuable electricity for use as green power supplies for next-generation electronics.

A popular candidate for a portable energy source that harvests energy from the environment is the triboelectric nanogenerator (TENG), first introduced by Wang et al. TENGs have many attractive features, including low fabrication costs, lightweight, high energy efficiency, and a wide range of materials and structures to choose from when designing a device,[7−9] leading to a large variety of viable device setups.[10−13] Among other factors, the contact area between the triboelectric layers plays a major role in determining the properties of a TENG.[14−19] Previous studies have focused on investigating the effects of material selection,[20−22] surface modification,[23−26] and surface morphology,[27−30] on the mechanism of operation and performance of TENGs. Because increasing the dielectric constant can enhance the capacitance of the dielectric layer, thereby increasing the surface charge density, the dielectric constant of a triboelectric material is an important factor affecting triboelectric performance.[31]

One particular drawback of the early TENG designs is the lack of flexibility of the involved materials that would be required for applications in next-generation electronics, including electronic skin, flexible and touch screen displays, electronic watches, and biomechanical monitoring sensors.[50−54] Consequently, extensive research has been undertaken to make the triboelectric layer—responsible for the generation of triboelectric charges in the TENG assembly—fully stretchable and reliable for wearable electronics.[54] Another challenge is fabricating flexible electrodes while still facilitating the transfer of charges to the external circuit with minimum loss. The influence of the mechanical flexibility of a wearable TENG on its output performance has been reported.[55,56] Apart from inherent material properties, it is also important to achieve high degrees of contact at the contact interface. Because of the generally insulating nature of

Received: November 14, 2022
Accepted: January 25, 2023
Published: February 9, 2023

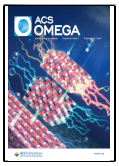

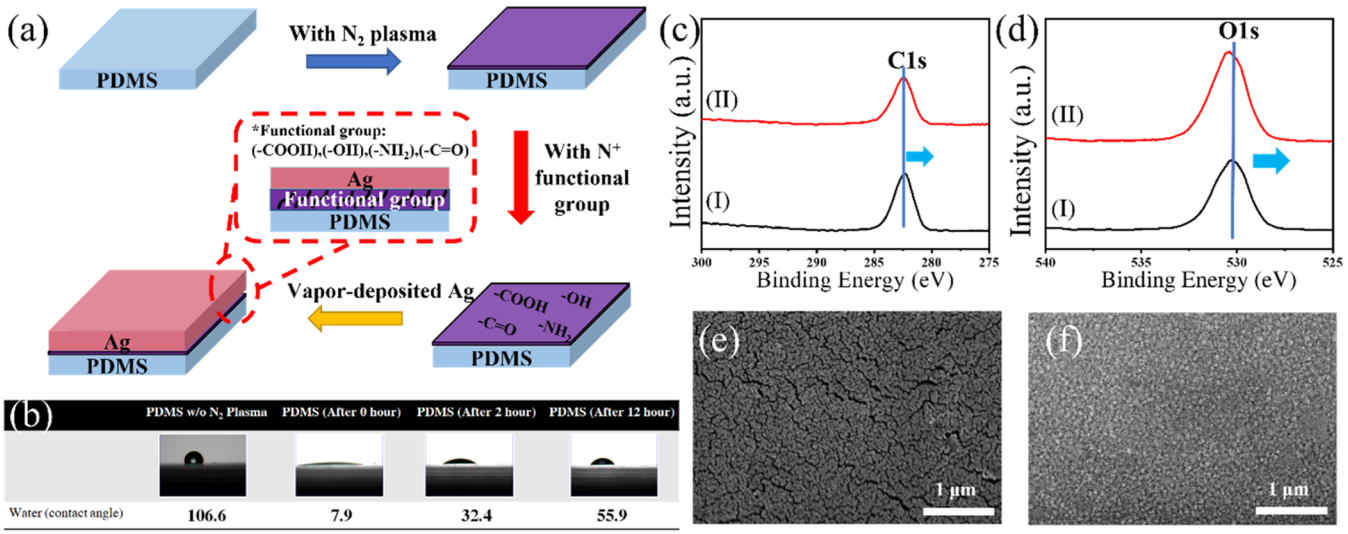

Figure 1. (a) Schematic representation of the surface modification of the stretchable electrode. (b) Contact-angle images of PDMS substrates before and after plasma treatment for 0, 2, and 12 h of exposure in the atmospheric environment. (c, d) X-ray photoelectron spectra (XPS) of the (c) C 1s and (d) O 1s binding energies of PDMS substrates prepared (I) without and (II) with N_2 treatment. (e, f) scanning electron microscopy (SEM) images of Ag films deposited on PDMS substrates prepared (e) without and (f) with N_2 treatment.

dielectric tribomaterials, charge transfer from the triboelectrification layer to the electrode (through electrostatic induction) in a TENG is of great concern. Therefore, appropriate engineering at the electrode surface and friction layer−electrode interface, along with optimization of the combination of electrodes with appropriate work functions and triboelectric materials, is required to ensure an increased surface charge density and power output.[57]

When selecting materials for TENGs with applications in wearable consumer electronics, there are other important aspects to consider. Traditional choices involved polymers, such as poly(tetrafluoroethylene) (PTFE), poly(vinylidene difluoride) (PVDF), polydimethylsiloxane (PDMS), and nylon, as friction layers, which are neither cost-effective nor biodegradable.[32−34] Furthermore, those commercial polymers can produce potentially harmful chemicals, restricting their applications in biomedicine. Hence, the development of bio-inspired, non-toxic, ultra-sensitive, and flexible TENGs has become a great challenge for next-generation biomedical applications.[35−38] Although several biowaste materials, including rice husks,[22] seagrasses,[39] leaves,[40,41] sunflower husks,[42] peanut shell powders,[43] and fish bladders,[44] have been used to form the friction layers, the processes for preparing biowaste material friction layers have been complicated and required the usage of harmful solvents. Moreover, those biowaste materials do not have a natural fiber structure, thereby minimizing the electrical output of the nanogenerator. A promising candidate for a biodegradable material with a natural fiber structure would be eggshell membranes (EMs).[45] EMs have been used as cost-efficient, eco-friendly, and flexible materials for printed electronic applications because they possess large numbers of COOH and NH_2 functional groups. For example, a highly efficient EM-based electrode material has been fabricated for supercapacitor applications.[46,47] In addition, EMs are capable of being piezoelectric, triboelectric, capacitive, and humidity sensing due to their nanofibrous structures and a variety of proteins within their structures.[48,49]

In this study, we used various types of EMs (hen, duck, goose, and ostrich) as positive friction materials to prepare stretchable electrodes for biodegradable TENGs. Among them, the output voltage of the ostrich EM could reach up to 300 V, due to its abundance of functional groups, natural fiber structure, high surface roughness, high surface charge, and high dielectric constant. The output power of the device reached 0.18 mW, sufficient to power 250 red light-emitting diodes simultaneously, as well as a digital watch. This ostrich EM-TENG not only exhibited excellent electrical properties, but we also used it as a smart sensor to detect body motion.

EXPERIMENTAL SECTION

EM Preparation. When buying eggs from the market, poke a small hole on the top of the egg and use tweezers to remove the eggshell to extract the membrane; then clean the membrane with DI water and dry it in an oven at 60 °C.

Surface Modification of a Stretchable Electrode. A PDMS (Dow Coring, Sylgard 184 A) solution was prepared by mixing 10:1 (w/w) monomer/curing agents to form the substrate. The PDMS solution was degassed under vacuum, and then cured at 60 °C for 1−2 h. A commercial N_2 plasma system (Harrick Plasma, PDC-32G) was used to modify the PDMS surface to form a hydrophilic surface layer. Thereafter, a Ag layer was formed on the PDMS surface through vapor deposition. The thickness of the Ag layer was approximately 50 nm, with a sheet resistance of approximately 1.34 Ω. A schematic representation of the surface modification of the stretchable electrode is displayed in Figure 1. The EM was peeled off with a thickness of 100−200 μm and a sample size of 2 cm × 2 cm.

Material Characterization. The chemical compositional changes to the PDMS surface after N_2 plasma treatment were analyzed using X-ray photoelectron spectroscopy (XPS, ULVAC-PHI). The sheet resistance of the Ag layer was measured using a four-point probe (Napson Corporation, RT-70V). The crystallinity of the EM was identified through X-ray diffraction (XRD) with Cu Kα radiation (λ = 1.5418 Å) at 30 kV and 20 mA at a scan rate of 2° min^{-1} from 5 to 40° (2θ). Field emission scanning electron microscopy (FE-SEM, Hitachi S-5200) operating at 2 kV was employed to determine

https://doi.org/10.1021/acsomega.2c07292
ACS Omega 2023, 8, 6699−6707

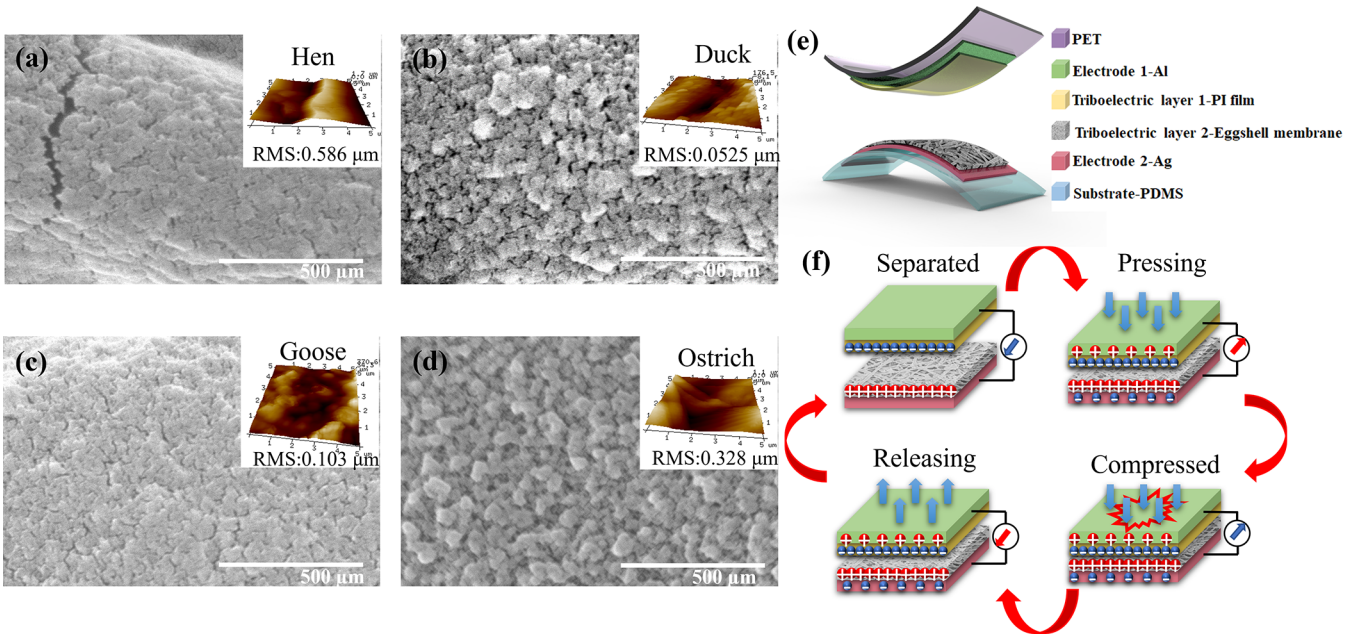

Figure 2. (a–d) SEM images of various types of EMs: (a) hen, (b) duck, (c) goose, and (d) ostrich. Insets: 3D views of the surface topographies. (e, f) Schematic representations of (e) the EM-TENG device and (f) the working mechanism of the EM contact-mode TENG.

the morphology of the EM and Ag layers. The surface roughnesses of the EMs were measured using an atomic force microscope (Bruker, Dimension Edge). The output voltages and currents from the bio-triboelectric devices were measured using an oscilloscope (Tektronix, DPO 3034). The dynamic mechanical pressure was applied using a magnetic shaker (Sinocera, Model JZK-20). The surface potential was measured using an electrostatic field meter (AccuraxS050C1). The dielectric constant was measured using a precision impedance analyzer (Microtest 6632). The surface charge was measured using a Keithley 6517B system electrometer (impedance: >200 TΩ).

RESULTS AND DISCUSSION

Figure 1a illustrates the procedure for preparing the plasma-treated PDMS substrate. First, a PDMS solution was fabricated by mixing the monomer and curing agent (mass ratio, 10:1) and degassing the mixture in a vacuum oven. The PDMS solution was then poured into a Petri dish and cured in a vacuum oven at 60 °C for 1–2 h to obtain the PDMS substrate. The surface-modified PDMS substrate was subjected to N_2 atmospheric plasma treatment to induce functional groups on the PDMS surface to form better connections. The N_2 plasma power is 18 W, and the N_2 pressure is 1.5 kgf/cm^2. PDMS surface roughness (rms) before and after N_2 plasma treatment is 0.834 and 0.289 nm, respectively. A layer of Ag was formed on the PDMS surface through vapor deposition. A Ag layer was also deposited on the surface of the untreated PDMS substrate (*i.e.*, without N_2 plasma treatment) to obtain corresponding Ag/PDMS substrates. The surfaces of the PDMS substrates were subjected to contact angle analysis (Figure 1b). The surface of the untreated PDMS substrate exhibited a water contact angle of 106.6°. After N_2 atmospheric plasma treatment, the contact angle decreased to 7.9°, indicating that the surface of this PDMS substrate was hydrophilic. Its contact angle increased from 7.9 to 55.9° after exposure to an atmospheric environment for 12 h, suggesting that the content of oxygen-containing functional groups on the plasma-treated surface of the PDMS substrate decreased upon increasing the exposure time.[58] Therefore, the plasma treatment of the PDMS substrate subjected to thermal evaporation must be performed within 1 h to avoid such a decrease in the availability of oxygen-containing functional groups. XPS revealed that the C 1s and O 1s peaks shifted after N_2 plasma treatment, indicating a strong connection between the Ag layer and PDMS (Figure 1c,d). We used SEM to investigate the morphologies of the Ag/PDMS substrates with and without plasma treatment (Figure 1e,f, respectively). The images revealed that relatively continuous 50-nm-thick Ag nanoparticle layers had been deposited on the PDMS substrates. For the unmodified PDMS substrate (Figure 1e), the surface morphology of the Ag nanoparticle layer featured isolated nanoparticles, potentially resulting in poor conductivity. After N_2 atmospheric plasma treatment, however, the morphology of the Ag nanoparticle layer changed to a relatively continuous layer (Figure 1f). Figure 1S (Supporting Information) presents SEM images of the Ag films deposited on PDMS substrates that had been subjected to various durations of N_2 plasma treatment.

Figure 2a–d presents the surface morphologies of the various types of EMs. Among them, the hen EM exhibited the highest roughness. The three-dimensional (3D) surface topographical image revealed that the surface of the hen EM was not flat, potentially resulting in lower electrical output due to poor draping with the friction layer. In contrast, the ostrich EM had greater roughness (RMS: 0.328 μm) but was a flat film that provided a large interspace and a high specific surface area, leading to efficient contact under pressure; moreover, it features unique and uniform particles on the fiber. Figure S2 displays SEM images of the various types of EMs, revealing their natural fiber structures with porosity on the contact surface, potentially helping to store more electrons in the pores, thereby prolonging the electrical output. We also used Fourier transform infrared (FTIR) spectroscopy to analyze the structures of the various types of EMs (Figure S3). The collagen fibrils in EMs are structurally stable because of their

https://doi.org/10.1021/acsomega.2c07292
ACS Omega 2023, 8, 6699–6707

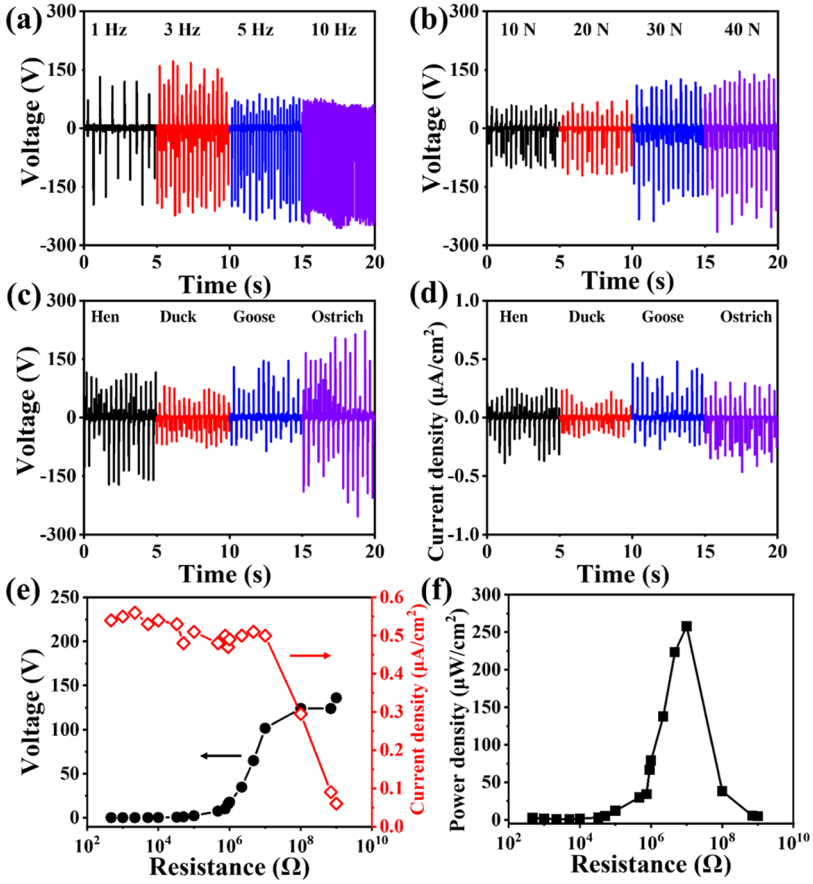

Figure 3. (a, b) Electrical output voltages of the various EMs measured at various (a) frequencies and (b) mechanical forces. (c) Maximum output voltages and (d) currents of the ostrich EM-TENG, measured at 30 N and 5 Hz. (e) Output voltage and current density, and (f) power density of the ostrich EM-TENG, plotted with respect to resistance.

regular chemical bonding and crystallinity. Figure 2e provides the schematic configuration of the EM-TENG device. For its fabrication, an EM was taken with a desired square shape (2.0 cm × 2.0 cm). One side of the selected EM portion was used as the positive tribomaterial, and the other was attached to a stretchable Ag electrode, which was used as the conducting electrode. We used a polyimide (PI) film as the negative tribomaterial, with conductive aluminum (Al) tape covering the PI surface as the electrode. Figure 2f presents an overview of the working principle of an EM-TENG in vertical contact−separation mode, involving a combination of triboelectrification and electrostatic induction. Prior to contact, no electron flow occurs in the separated model. Once an external force is applied to bring the EM and Kapton into contact, surface charge transfer occurs at the interface due to a triboelectric effect. The direction of the charge transfer is determined by the relative triboelectric polarity of the two layers. In this study, we used Kapton as the negative triboelectric material due to its triboelectric polarity. When the external force is released, the EM and Kapton surfaces become separated. At this stage, the separation of the surface charges leads to an increasingly strong dipole moment, creating an electric potential difference between the electrodes. As a consequence, electrons begin to flow from a negative to positive potential, with charges accumulating on the electrodes, resulting in a positive electrical signal. Several physical properties of triboelectric materials—in particular, their surface roughness, electron affinity, friction, and dielectric constant—affect the performance of TENGs. Among them, a high dielectric constant is the most important property for improving the output performance of the devices, measured in terms of their output voltages and currents.[6,27]

We measured the electrical properties of the ostrich EM-TENG while varying the operating frequency, applied force, and external load. Figure 3a,b displays the electrical output voltages of the ostrich EM at various frequencies and mechanical forces, respectively. When the frequency was varied from 1 to 3 Hz under an applied force of 30 N, the peak output voltage for the ostrich EM mats increased from approximately 280 V to approximately 300 V (Figure 3a). Increasing the operating frequency resulted in more intense friction, which generated more charges due to faster contact between the ostrich EM and the Kapton layer. Nevertheless, the output voltage became unstable at frequencies greater than 5−10 Hz. This instability arose because, at these high frequencies, the contact and separation processes of the triboelectric layers were incomplete, preventing the surface charge from reaching its maximum value. With a fixed operating frequency of 3 Hz, the output voltage of the ostrich EM increased from approximately 150 V to approximately 300 V upon increasing the applied force from 10 to 40 N. This behavior presumably resulted from an increased compressive force, leading to significantly improved contact between the triboelectric layers, thereby resulting in the generation of more electric charges. The output voltage was almost saturated, however, when the compressive force was greater than 30 N. Thus, the optimized conditions for subsequent studies

https://doi.org/10.1021/acsomega.2c07292
ACS Omega 2023, 8, 6699−6707

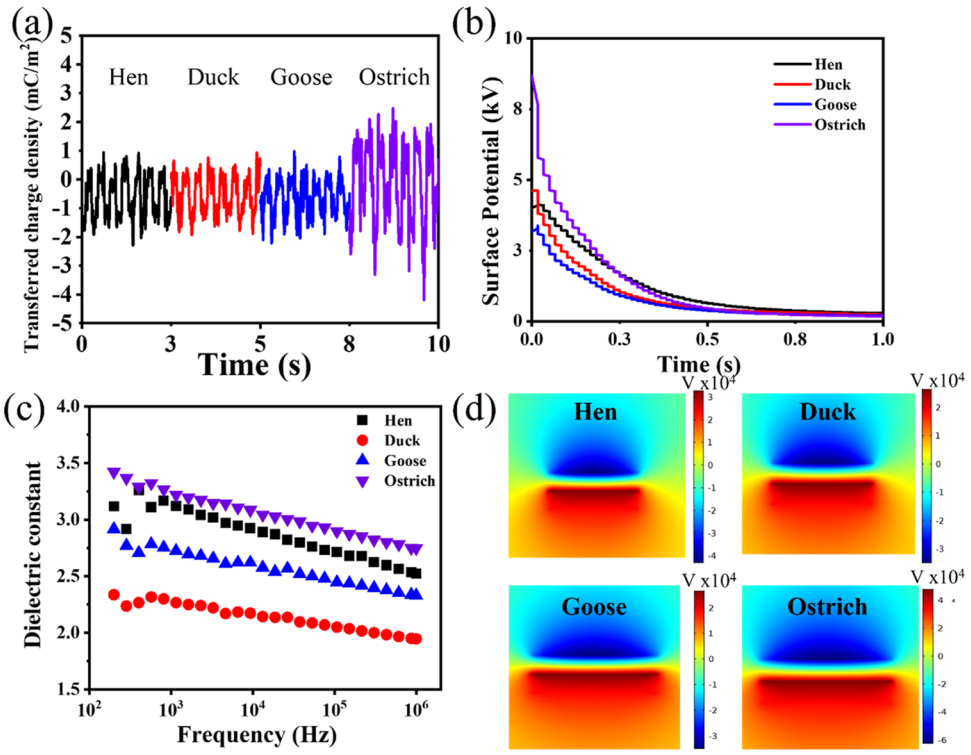

Figure 4. (a) Transferred charges and (b) retention times of the surface potentials for various types of EMs after contact friction with a Kapton film. (c) Dielectric constants for the various types of EMs. (d) Finite-element simulation of the electric potential variation for the various types of EMs.

involved a cycled compressive force of 30 N at an applied frequency of 3 Hz. Figure S4 provides the electrical output currents of the ostrich EM measured at various frequencies and mechanical forces. Figure 3c displays the maximum output performance data of the various EMs under a cycled compressive force of 30 N at an applied frequency of 3 Hz. The output voltages of the hen, duck, goose, and ostrich EMs were approximately 250, 150, 200, and 300 V, respectively, under the same mechanical force. The output current density of the ostrich EM reached up to approximately 0.6 μA/cm^2, higher than those of the duck and goose EMs (Figure 3d). The combination of the open-circuit voltage and short-circuit current led to the maximal power of the ostrich EM (18 mW) being greater than those achievable for the hen, duck, and goose EMs alone (17.5, 4.5, and 8.0 mW, respectively). Furthermore, Figure 3e,f presents the measured voltage outputs, current outputs, and power densities generated by the ostrich EM-TENG under various external load resistances when operated at 3 Hz and 40 N. The output voltage increased upon increasing the external load resistance from 470 Ω to 1 MΩ, with the output current decreasing until the external load resistance reached 10 MΩ. Consequently, the ostrich EM-TENG exhibited a maximum output power density of 270 μW/cm^2 at a resistance of 10 MΩ. Figure 5S provides the measured voltage outputs, current outputs, and power densities generated by the hen, duck, and goose EM-TENG under various external load resistances. Compared with the hen EM-TENG, the power density of the ostrich EM-TENG was 1.1 times higher, due to its higher surface roughness, surface charge, surface potential, and dielectric constant.

Several studies have revealed that the surface charge density can be enhanced by incorporating microscopic structures or engineering functional groups onto the surfaces of triboelectric materials.[27,57,59,60] Figure 4a reveals the amounts of charge transferred for the various types of EMs. Among them, the ostrich EM possessed the highest amount of transferred charge due to its good contact area and surface roughness (as determined using SEM and AFM), thereby generating more electrons through friction when compared with the other various EMs. Moreover, the maximum transferred charge in the ostrich EM suggests improvements in the capture and storage of the triboelectric electrons, thereby enhancing the electrical output. The initial surface potentials of the hen, duck, goose, and ostrich EMs were approximately 4.5, 4.7, 3.0, and 9.5 kV, respectively. Among them, the ostrich EM had the highest initial surface potential, indicating that its highest surface charge would result in the highest electrical output. According to the relationship between the transferred charge and the dynamic capacitance of a TENG, the first derivative of the charge with respect to time can be expressed as

$$\frac{dQ_{sc}}{dt} = V_{oc}(x)\frac{dC(x)}{dt} + C(x)\frac{dV_{oc}(x)}{dt} \quad (1)$$

Equation 1 indicates that the rate at which the capacitance changes with respect to time is a critical parameter. Hence, the output performance can be optimized by changing the dielectric film's compressibility, for example, by incorporating porous sponge structures into triboelectric materials. Figure 4c plots the dielectric constants for the various eggshell membranes with respect to frequency. All EMs exhibited a dielectric constant of approximately 3 at a frequency of 10 kHz. Nevertheless, the overall dielectric constant of the EM was small because of its porous nature. The dielectric constant of each of the four EMs decreased upon increasing the frequency, possibly due to a polarization effect. When the frequency becomes too high, reorientation of the dipoles becomes

https://doi.org/10.1021/acsomega.2c07292
ACS Omega 2023, 8, 6699−6707

impossible, causing the dielectric constant to decrease toward 1.0, close to the dielectric constant of air.[61] As displayed in Figure 4c, the dielectric constant of the ostrich EM was higher than those of the others, due to a lower volume of pores (Table 1) and a higher amount of transferred charge. The surface charge densities and dielectric constants of triboelectric materials are known to impact the output performance of TENGs.[59,60] In this study of four different kinds of EM-TENGs, we used the finite-element simulation tool (COMSOL multiphysics) to calculate the electric potentials of the EM-TENGs (Figure 4d). The distance between the two triboelectric materials was set at 3 mm. For the hen, duck, goose, and ostrich EM-TENGs, the measured triboelectric charges were 0.80, 0.65, 0.65, and 1.17 mC/m^2, respectively, with dielectric constants of 2.81, 2.15, 2.57, and 3.05, respectively, used for simulation of the electric potential. Because of the influence of the relative permittivity, the material with the lower relative permittivity would be negatively charged, while the other triboelectric material would be positively charged. We found that the ostrich EM possessed the highest surface charge and dielectric constant, resulting in the highest electrical output.

Table 1. (a) SEM-derived data for pore sizes and fiber sizes; and (b) Brunauer−Emmett−Teller (BET)-derived data for surface areas and pore volumes of the hen, duck, goose, and ostrich EMs

analysis	item	a. Hen	b. Duck	c. Goose	d. Ostrich
(a) SEM	pore size (μm)	3.8	3.9	8.0	3.9
	fiber size (μm)	1.5	1.6	1.9	2.7
(b) BET	BET surface area (m^2/g)	1.51	1.84	1.29	1.17
	pore volume (cm^3/g)	0.000573	0.00121	0.000546	0.00133

A device's robustness is also critical to its output performance. The wear that occurs to an EM-TENG device after long hours of operation will cause its output to be unstable, gradually degrading. To examine the mechanical stability of the optimal EM-TENG device, we monitored the electrical output of the ostrich EM-TENG over a duration of 9000 cycles at 40 N with a frequency of 3 Hz (Figure 5a), revealing the high durability and stability of the ostrich EM-TENG. Figure 5b displays the voltage curves obtained when charging capacitors of varying capacitance (0.1, 1.0, 2.2, 4.7, and 10 μF) with an ostrich EM-TENG, with the 0.1 μF capacitor undergoing charging to 6.5 V within 37 s. Furthermore, an LED bulb array and a digital watch could be powered by the EM-TENG, as displayed in Movie S1. Moreover, the ostrich EM-TENG device could be used not only as a self-powering device but also as a sensor. We employed this EM-TENG to detect leg movement by attaching it to a leg (Figure 5d, Movie S2). During leg movement, the ostrich EM-TENG generated an output signal that varied based on the speed of motion. In another instance, we assessed the sensitivity of the ostrich EM-TENG by varying the number of fingers pressed onto the device (Figure 5e). Interestingly, the shape of the output signal, namely the number of peaks, changed depending on the number of fingers pressing on the device. We also successfully implemented the fabricated EM-TENG sensor to detect air blowing from a mouth (Figure 5f), suggesting that this EM-TENG could be used to harvest wind energy. Accordingly, this ostrich EM-TENG device has potential for several applications in monitoring human actions and as a power source.

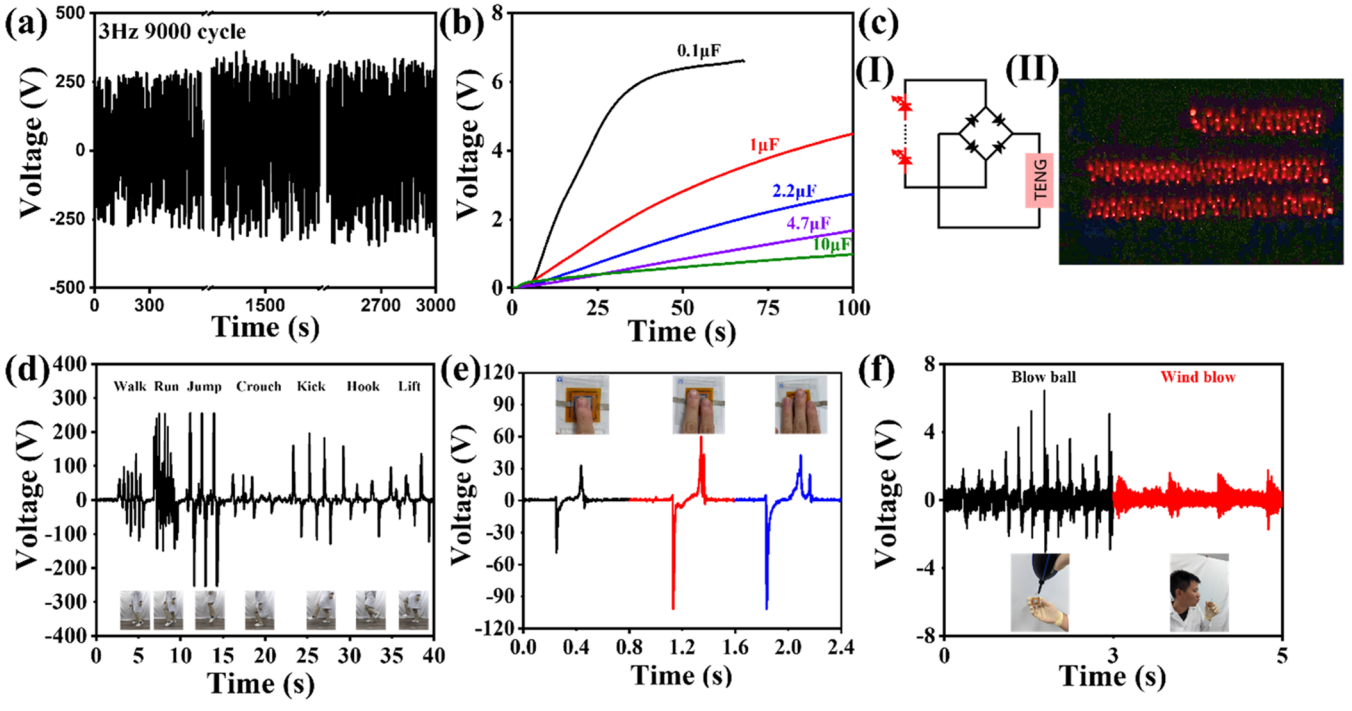

Figure 5. (a) Electrical outputs during long-term cycling of the ostrich EM-TENG. (b) Using the ostrich EM-TENG to charge capacitors of various capacitances. (b) (I) Schematic representation of the operating circuit for LED bulbs with a full-wave bridge rectifier and (II) photograph of 250 serially connected LEDs powered by a TENG formed from ostrich EMs (device size: 2.5 cm × 2.5 cm). (d−f) Sensitivity of the ostrich EM-TENG, measured by (d) leg movement, (e) varying the number of fingers pressing on the device, and (f) air blowing.

https://doi.org/10.1021/acsomega.2c07292
ACS Omega 2023, 8, 6699−6707

CONCLUSIONS

We have investigated four types of EMs as friction materials with stretchable electrodes. Among them, the ostrich EM displayed the highest electrical output due to its abundance of functional groups, natural fiber structure, high surface roughness, high surface charge, and high dielectric constant. The optimized and fabricated ostrich EM-TENG exhibited output powers of up to 0.18 mW, sufficient to operate 250 red LEDs instantaneously. Furthermore, this device could generate power effectively under various external resistance loads. The output voltage of the EM-TENG was stable during long-term cycling. Furthermore, we found that the ostrich EM-TENG could be used as a smart sensor, with applications in a wide range of wearable electronics: for powering various small-scale electronic devices, in biomedical monitoring systems, or for sensing mechanical motions. The electrospinning method is a nanofiber fabrication technology. Other varieties of triboelectric nanofiber materials could be fabricated using the electrospinning method.

ASSOCIATED CONTENT

Supporting Information

The Supporting Information is available free of charge at https://pubs.acs.org/doi/10.1021/acsomega.2c07292.

SEM images, FTIR spectra (PDF)

Movie S1 LED bulb array and a digital watch (MP4)

Movie S2 body motion (MP4)

AUTHOR INFORMATION

Corresponding Authors

Meng-Fang Lin − *Department of Materials Engineering, Ming Chi University of Technology, New Taipei City 24301, Taiwan; Center for Plasma and Thin Film Technologies and Research Center for Intelligent Medical Devices, Ming Chi University of Technology, New Taipei City 24301, Taiwan;* orcid.org/0000-0002-9286-6527; Email: mflin@mail.mcut.edu.tw

Chih-Ping Chen − *Department of Materials Engineering, Ming Chi University of Technology, New Taipei City 24301, Taiwan; Center for Plasma and Thin Film Technologies, Ming Chi University of Technology, New Taipei City 24301, Taiwan;* orcid.org/0000-0002-0281-7554; Email: cpchen@mail.mcut.edu.tw

Authors

Po-Yen Chang − *Department of Materials Engineering, Ming Chi University of Technology, New Taipei City 24301, Taiwan; Center for Plasma and Thin Film Technologies, Ming Chi University of Technology, New Taipei City 24301, Taiwan; Institute of Polymer Science and Engineering, National Taiwan University, Taipei 106, Taiwan*

Chia-Hsien Lee − *Department of Materials Engineering, Ming Chi University of Technology, New Taipei City 24301, Taiwan; Center for Plasma and Thin Film Technologies, Ming Chi University of Technology, New Taipei City 24301, Taiwan*

Xin-Xian Wu − *Department of Materials Engineering, Ming Chi University of Technology, New Taipei City 24301, Taiwan; Center for Plasma and Thin Film Technologies, Ming Chi University of Technology, New Taipei City 24301, Taiwan*

Ru-Jong Jeng − *Institute of Polymer Science and Engineering, National Taiwan University, Taipei 106, Taiwan;* orcid.org/0000-0002-0913-4975

Complete contact information is available at: https://pubs.acs.org/10.1021/acsomega.2c07292

Notes

The authors declare no competing financial interest.

ACKNOWLEDGMENTS

The authors would like to thank the Ministry of Science and Technology (NSTC 111-2221-131-019-MY3) and the Ministry of Education of Taiwan (E01-111-023) for financially supporting this research.

REFERENCES

(1) Romero, E.; Novoderezhkin, V. I.; van Grondelle, R. Quantum design of photosynthesis for bio-inspired solar-energy conversion. *Nature* **2017**, *543*, 355−365.

(2) Islam, M. R.; Mekhilef, S.; Saidur, R. Progress and recent trends of wind energy technology. *Renewable Sustainable Energy Rev.* **2013**, *21*, 456−468.

(3) Liu, G.; Guo, H.; Xu, S.; Hu, C.; Wang, Z. L. Oblate Spheroidal Triboelectric Nanogenerator for All-Weather Blue Energy Harvesting. *Adv. Energy Mater.* **2019**, *9*, No. 1900801.

(4) Wang, J.; He, J.; Ma, L.; Zhang, Y.; Shen, L.; Xiong, S.; Li, K.; Qu, M. Multifunctional conductive cellulose fabric with flexibility, superamphiphobicity and flame-retardancy for all-weather wearable smart electronic textiles and high-temperature warning device. *Chem. Eng. J.* **2020**, *390*, No. 124508.

(5) Sah, D. K.; Amgoth, T. Renewable energy harvesting schemes in wireless sensor networks: A Survey. *Inf. Fusion* **2020**, *63*, 223−247.

(6) Fan, F.-R.; Tian, Z.-Q.; Lin Wang, Z. Flexible triboelectric generator. *Nano Energy* **2012**, *1*, 328−334.

(7) Wang, Z. L. Nanogenerators, self-powered systems, blue energy, piezotronics and piezo-phototronics − A recall on the original thoughts for coining these fields. *Nano Energy* **2018**, *54*, 477−483.

(8) Chen, J.; Wang, Z. L. Reviving Vibration Energy Harvesting and Self-Powered Sensing by a Triboelectric Nanogenerator. *Joule* **2017**, *1*, 480−521.

(9) Wang, Z. L. Triboelectric nanogenerators as new energy technology and self-powered sensors − Principles, problems and perspectives. *Faraday Discuss.* **2014**, *176*, 447−458.

(10) Cheng, P.; Liu, Y.; Wen, Z.; Shao, H.; Wei, A.; Xie, X.; Chen, C.; Yang, Y.; Peng, M.; Zhuo, Q.; Sun, X. Atmospheric pressure difference driven triboelectric nanogenerator for efficiently harvesting ocean wave energy. *Nano Energy* **2018**, *54*, 156−162.

(11) Kim, J.; Ryu, H.; Lee, J. H.; Khan, U.; Kwak, S. S.; Yoon, H.-J.; Kim, S.-W. High Permittivity CaCu3Ti4O12 Particle-Induced Internal Polarization Amplification for High Performance Triboelectric Nanogenerators. *Adv. Energy Mater.* **2020**, *10*, No. 1903524.

(12) Rodrigues, C.; Nunes, D.; Clemente, D.; Mathias, N.; Correia, J. M.; Rosa-Santos, P.; Taveira-Pinto, F.; Morais, T.; Pereira, A.; Ventura, J. Emerging triboelectric nanogenerators for ocean wave energy harvesting: state of the art and future perspectives. *Energy Environ. Sci.* **2020**, *13*, 2657−2683.

(13) Zheng, Q.; Shi, B.; Li, Z.; Wang, Z. L. Recent Progress on Piezoelectric and Triboelectric Energy Harvesters in Biomedical Systems. *Adv. Sci.* **2017**, *4*, No. 1700029.

(14) Khandelwal, G.; Maria Joseph Raj, N. P.; Kim, S.-J. Zeolitic Imidazole Framework: Metal−Organic Framework Subfamily Members for Triboelectric Nanogenerators. *Adv. Funct. Mater.* **2020**, *30*, No. 1910162.

(15) Wang, Y.; Duan, J.; Yang, X.; Liu, L.; Zhao, L.; Tang, Q. The unique dielectricity of inorganic perovskites toward high-performance triboelectric nanogenerators. *Nano Energy* **2020**, *69*, No. 104418.

(16) Cao, V. A.; Lee, S.; Kim, M.; Alam, M. M.; Park, P.; Nah, J. Output power density enhancement of triboelectric nanogenerators via ferroelectric polymer composite interfacial layers. *Nano Energy* **2020**, *67*, No. 104300.
(17) Zhao, P.; Soin, N.; Kumar, A.; Shi, L.; Guan, S.; Tsonos, C.; Yu, Z.; Ray, S. C.; McLaughlin, J. A.; Zhu, Z.; Zhou, E.; Geng, J.; See, C. H.; Luo, J. Expanding the portfolio of tribo-positive materials: Aniline formaldehyde condensates for high charge density triboelectric nanogenerators. *Nano Energy* **2020**, *67*, No. 104291.
(18) Gao, L.; Chen, X.; Lu, S.; Zhou, H.; Xie, W.; Chen, J.; Qi, M.; Yu, H.; Mu, X.; Wang, Z. L.; Yang, Y. Triboelectric Nanogenerators: Enhancing the Output Performance of Triboelectric Nanogenerator via Grating-Electrode-Enabled Surface Plasmon Excitation (Adv. Energy Mater. 44/2019). *Adv. Energy Mater.* **2019**, *9*, No. 1970177.
(19) Li, Z.; Zhao, L.; Zheng, X.; Lin, P.; Li, X.; Li, R.; Han, D.; Zhao, S.; Lv, D.; Wang, L.; Wang, X.; Zhao, Y. Continuous PEDOT:PSS nanomesh film: Towards aqueous AC line filtering capacitor with ultrahigh energy density. *Chem. Eng. J.* **2022**, *430*, No. 133012.
(20) Kim, Y. J.; Lee, J.; Park, S.; Park, C.; Park, C.; Choi, H.-J. Effect of the relative permittivity of oxides on the performance of triboelectric nanogenerators. *RSC Adv.* **2017**, *7*, 49368−49373.
(21) Zhao, X. J.; Zhu, G.; Wang, Z. L. Coplanar Induction Enabled by Asymmetric Permittivity of Dielectric Materials for Mechanical Energy Conversion. *ACS Appl. Mater. Interfaces* **2015**, *7*, 6025−6029.
(22) Wu, J. M.; Chang, C. K.; Chang, Y. T. High-output current density of the triboelectric nanogenerator made from recycling rice husks. *Nano Energy* **2016**, *19*, 39−47.
(23) Wang, S.; Zi, Y.; Zhou, Y. S.; Li, S.; Fan, F.; Lin, L.; Wang, Z. L. Molecular surface functionalization to enhance the power output of triboelectric nanogenerators. *J. Mater. Chem. A* **2016**, *4*, 3728−3734.
(24) Byun, K.-E.; Cho, Y.; Seol, M.; Kim, S.; Kim, S.-W.; Shin, H.-J.; Park, S.; Hwang, S. Control of Triboelectrification by Engineering Surface Dipole and Surface Electronic State. *ACS Appl. Mater. Interfaces* **2016**, *8*, 18519−18525.
(25) Wu, C.; Kim, T. W.; Choi, H. Y. Reduced graphene-oxide acting as electron-trapping sites in the friction layer for giant triboelectric enhancement. *Nano Energy* **2017**, *32*, 542−550.
(26) Song, G.; Kim, Y.; Yu, S.; Kim, M.-O.; Park, S.-H.; Cho, S. M.; Velusamy, D. B.; Cho, S. H.; Kim, K. L.; Kim, J.; Kim, E.; Park, C. Molecularly Engineered Surface Triboelectric Nanogenerator by Self-Assembled Monolayers (METS). *Chem. Mater.* **2015**, *27*, 4749−4755.
(27) Fan, F.-R.; Lin, L.; Zhu, G.; Wu, W.; Zhang, R.; Wang, Z. L. Transparent Triboelectric Nanogenerators and Self-Powered Pressure Sensors Based on Micropatterned Plastic Films. *Nano Lett.* **2012**, *12*, 3109−3114.
(28) Jeong, C. K.; Baek, K. M.; Niu, S.; Nam, T. W.; Hur, Y. H.; Park, D. Y.; Hwang, G.-T.; Byun, M.; Wang, Z. L.; Jung, Y. S.; Lee, K. J. Topographically-Designed Triboelectric Nanogenerator via Block Copolymer Self-Assembly. *Nano Lett.* **2014**, *14*, 7031−7038.
(29) Lin, Z.-H.; Xie, Y.; Yang, Y.; Wang, S.; Zhu, G.; Wang, Z. L. Enhanced Triboelectric Nanogenerators and Triboelectric Nanosensor Using Chemically Modified TiO2 Nanomaterials. *ACS Nano* **2013**, *7*, 4554−4560.
(30) Wang, S.; Lin, L.; Wang, Z. L. Nanoscale Triboelectric-Effect-Enabled Energy Conversion for Sustainably Powering Portable Electronics. *Nano Lett.* **2012**, *12*, 6339−6346.
(31) Kim, M. P.; Um, D.-S.; Shin, Y.-E.; Ko, H. High-Performance Triboelectric Devices via Dielectric Polarization: A Review. *Nanoscale Res. Lett.* **2021**, *16*, No. 35.
(32) Yang, Y.; Zhu, G.; Zhang, H.; Chen, J.; Zhong, X.; Lin, Z.-H.; Su, Y.; Bai, P.; Wen, X.; Wang, Z. L. Triboelectric Nanogenerator for Harvesting Wind Energy and as Self-Powered Wind Vector Sensor System. *ACS Nano* **2013**, *7*, 9461−9468.
(33) Chen, S. W.; Cao, X.; Wang, N.; Ma, L.; Zhu, H. R.; Willander, M.; Jie, Y.; Wang, Z. L. An Ultrathin Flexible Single-Electrode Triboelectric-Nanogenerator for Mechanical Energy Harvesting and Instantaneous Force Sensing. *Adv. Energy Mater.* **2017**, *7*, No. 1601255.
(34) Zheng, Y.; Cheng, L.; Yuan, M.; Wang, Z.; Zhang, L.; Qin, Y.; Jing, T. An electrospun nanowire-based triboelectric nanogenerator and its application in a fully self-powered UV detector. *Nanoscale* **2014**, *6*, 7842−7846.
(35) Yang, M.; Tian, X.; Hua, T. Green and recyclable cellulose based TENG for sustainable energy and human-machine interactive system. *Chem. Eng. J.* **2022**, *442*, No. 136150.
(36) Bo, X.; Uyanga, K. A.; Wang, L.; Firdous, I.; Shi, J.; Li, W.; Almardi, J. M.; Fahim, M.; Liu, F.; Lyu, H.; Daoud, W. A. High power-output and highly stretchable protein-based biomechanical energy harvester. *Chem. Eng. J.* **2023**, *451*, No. 138714.
(37) Zhou, Z.; Li, X.; Wu, Y.; Zhang, H.; Lin, Z.; Meng, K.; Lin, Z.; He, Q.; Sun, C.; Yang, J.; Wang, Z. L. Wireless self-powered sensor networks driven by triboelectric nanogenerator for in-situ real time survey of environmental monitoring. *Nano Energy* **2018**, *53*, 501−507.
(38) Xia, K.; Zhu, Z.; Fu, J.; Li, Y.; Chi, Y.; Zhang, H.; Du, C.; Xu, Z. A triboelectric nanogenerator based on waste tea leaves and packaging bags for powering electronic office supplies and behavior monitoring. *Nano Energy* **2019**, *60*, 61−71.
(39) Saqib, Q. M.; Chougale, M. Y.; Khan, M. U.; Shaukat, R. A.; Kim, J.; Bae, J.; Lee, H. W.; Park, J.-I.; Kim, M. S.; Lee, B. G. Natural seagrass tribopositive material based spray coatable triboelectric nanogenerator. *Nano Energy* **2021**, *89*, No. 106458.
(40) Jie, Y.; Jia, X.; Zou, J.; Chen, Y.; Wang, N.; Wang, Z. L.; Cao, X. Natural Leaf Made Triboelectric Nanogenerator for Harvesting Environmental Mechanical Energy. *Adv. Energy Mater.* **2018**, *8*, No. 1703133.
(41) Feng, Y.; Zhang, L.; Zheng, Y.; Wang, D.; Zhou, F.; Liu, W. Leaves based triboelectric nanogenerator (TENG) and TENG tree for wind energy harvesting. *Nano Energy* **2019**, *55*, 260−268.
(42) Shaukat, R. A.; Saqib, Q. M.; Khan, M. U.; Chougale, M. Y.; Bae, J. biowaste sunflower husks powder based recycled triboelectric nanogenerator for energy harvesting. *Energy Rep.* **2021**, *7*, 724−731.
(43) Saqib, Q. M.; Shaukat, R. A.; Khan, M. U.; Chougale, M.; Bae, J. Biowaste Peanut Shell Powder-Based Triboelectric Nanogenerator for Biomechanical Energy Scavenging and Sustainably Powering Electronic Supplies. *ACS Appl. Electron. Mater.* **2020**, *2*, 3953−3963.
(44) Ma, J.; Zhu, J.; Ma, P.; Jie, Y.; Wang, Z. L.; Cao, X. Fish Bladder Film-Based Triboelectric Nanogenerator for Noncontact Position Monitoring. *ACS Energy Lett.* **2020**, *5*, 3005−3011.
(45) Liu, X.; Yin, C.; Yang, J.; Liang, M.; Wei, J.; Zhang, Z.; Wang, H.; Wang, Q. Controllable preparation of an eggshell membrane supported hydrogel electrolyte with thickness-dependent electrochemical performance. *J. Mater. Chem. A* **2016**, *4*, 17933−17938.
(46) Li, Z.; Zhang, L.; Amirkhiz, B. S.; Tan, X.; Xu, Z.; Wang, H.; Olsen, B. C.; Holt, C. M. B.; Mitlin, D. Carbonized Chicken Eggshell Membranes with 3D Architectures as High-Performance Electrode Materials for Supercapacitors. *Adv. Energy Mater.* **2012**, *2*, 431−437.
(47) Geng, J.; Wu, H.; Al-Enizi, A. M.; Elzatahry, A. A.; Zheng, G. Freestanding eggshell membrane-based electrodes for high-performance supercapacitors and oxygen evolution reaction. *Nanoscale* **2015**, *7*, 14378−14384.
(48) Saqib, Q. M.; Khan, M. U.; Bae, J. Inner egg shell membrane based bio-compatible capacitive and piezoelectric function dominant self-powered pressure sensor array for smart electronic applications. *RSC Adv.* **2020**, *10*, 29214−29227.
(49) Yan, S.; Zhang, Z.; Shi, X.; Xu, Y.; Li, Y.; Wang, X.; Li, Q.; Turng, L.-S. Eggshell membrane and expanded polytetrafluoroethylene piezoelectric-enhanced triboelectric bio-nanogenerators for energy harvesting. *Int. J. Energy Res.* **2021**, *45*, 11053−11064.
(50) Zhao, S.; Li, J.; Cao, D.; Zhang, G.; Li, J.; Li, K.; Yang, Y.; Wang, W.; Jin, Y.; Sun, R.; Wong, C.-P. Recent Advancements in Flexible and Stretchable Electrodes for Electromechanical Sensors: Strategies, Materials, and Features. *ACS Appl. Mater. Interfaces* **2017**, *9*, 12147−12164.
(51) Wen, Z.; Yang, Y.; Sun, N.; Li, G.; Liu, Y.; Chen, C.; Shi, J.; Xie, L.; Jiang, H.; Bao, D.; Zhuo, Q.; Sun, X. A Wrinkled PEDOT:PSS Film Based Stretchable and Transparent Triboelectric Nanogenerator

https://doi.org/10.1021/acsomega.2c07292
ACS Omega 2023, 8, 6699−6707

for Wearable Energy Harvesters and Active Motion Sensors. *Adv. Funct. Mater.* **2018**, *28*, No. 1803684.
(52) Doganay, D.; Cicek, M. O.; Durukan, M. B.; Altuntas, B.; Agbahca, E.; Coskun, S.; Unalan, H. E. Fabric based wearable triboelectric nanogenerators for human machine interface. *Nano Energy* **2021**, *89*, No. 106412.
(53) Sun, J.; Pu, X.; Liu, M.; Yu, A.; Du, C.; Zhai, J.; Hu, W.; Wang, Z. L. Self-Healable, Stretchable, Transparent Triboelectric Nanogenerators as Soft Power Sources. *ACS Nano* **2018**, *12*, 6147−6155.
(54) Shi, M.; Wu, H.; Zhang, J.; Han, M.; Meng, B.; Zhang, H. Self-powered wireless smart patch for healthcare monitoring. *Nano Energy* **2017**, *32*, 479−487.
(55) Xu, C.; Zhang, B.; Wang, A. C.; Zou, H.; Liu, G.; Ding, W.; Wu, C.; Ma, M.; Feng, P.; Lin, Z.; Wang, Z. L. Contact-Electrification between Two Identical Materials: Curvature Effect. *ACS Nano* **2019**, *13*, 2034−2041.
(56) Lai, Y.-C.; Deng, J.; Niu, S.; Peng, W.; Wu, C.; Liu, R.; Wen, Z.; Wang, Z. L. Electric Eel-Skin-Inspired Mechanically Durable and Super-Stretchable Nanogenerator for Deformable Power Source and Fully Autonomous Conformable Electronic-Skin Applications. *Adv. Mater.* **2016**, *28*, 10024−10032.
(57) Kim, D. W.; Lee, J. H.; Kim, J. K.; Jeong, U. Material aspects of triboelectric energy generation and sensors. *NPG Asia Mater.* **2020**, *12*, No. 6.
(58) Qin, W.; Meng, J.; Wang, Y. Effect of cold plasma process on the surface wettability of NBR and the kerosene resistance of NBR/PTFE composites. *Surf. Interface Anal.* **2017**, *49*, 1008−1016.
(59) Yang, H.; Fan, F. R.; Xi, Y.; Wu, W. Design and engineering of high-performance triboelectric nanogenerator for ubiquitous unattended devices. *EcoMat* **2021**, *3*, No. e12093.
(60) Yu, A.; Zhu, Y.; Wang, W.; Zhai, J. Progress in Triboelectric Materials: Toward High Performance and Widespread Applications. *Adv. Funct. Mater.* **2019**, *29*, No. 1900098.
(61) Etuk, S. E.; Robert, U. W.; Emah, J. B.; Agbasi, O. E. Dielectric Properties of Eggshell Membrane of Some Select Bird Species. *Arab. J. Sci. Eng.* **2021**, *46*, 769−777.

https://doi.org/10.1021/acsomega.2c07292
ACS Omega 2023, 8, 6699−6707